

# Clinical Myocardial Perfusion PET/CT\*

Marcelo F. Di Carli<sup>1-3</sup>, Sharmila Dorbala<sup>1-3</sup>, Jolene Meserve<sup>1</sup>, Georges El Fakhri<sup>1</sup>, Arkadiusz Sitek<sup>1</sup>, and Stephen C. Moore<sup>1</sup>

<sup>1</sup>Division of Nuclear Medicine/PET, Department of Radiology, Brigham and Women's Hospital, Harvard Medical School, Boston, Massachusetts; <sup>2</sup>Division of Cardiovascular Imaging, Department of Radiology, Brigham and Women's Hospital, Harvard Medical School, Boston, Massachusetts; and <sup>3</sup>Division of Cardiology, Department of Medicine, Brigham and Women's Hospital, Harvard Medical School, Boston, Massachusetts

The field of nuclear cardiology is witnessing growing interest in the use of cardiac PET for the evaluation of patients with coronary artery disease (CAD). The available evidence suggests that myocardial perfusion PET provides an accurate means for diagnosing obstructive CAD, which appears superior to SPECT especially in the obese and in those undergoing pharmacologic stress. The ability to record changes in left ventricular function from rest to peak stress and to quantify myocardial perfusion (in mL/min/g of tissue) provides an added advantage over SPECT for evaluating multivessel CAD. There is growing and consistent evidence that gated myocardial perfusion PET also provides clinically useful risk stratification. Although the introduction of hybrid PET/CT technology offers the exciting possibility of assessing the extent of anatomic CAD (CT coronary angiography) and its functional consequences (ischemic burden) in the same setting, there are technical challenges in the implementation of CT-based transmission imaging for attenuation correction. Nonetheless, this integrated platform for assessing anatomy and biology offers a great potential for translating advances in molecularly targeted imaging into humans.

**Key Words:** myocardial perfusion imaging; PET/CT; CT angiography; cardiac PET

**J Nucl Med 2007; 48:783-793**

DOI: 10.2967/jnumed.106.032789

**P**ET has contributed significantly to advance our understanding of heart physiology and pathophysiology for >25 y. Initially, it emerged as a powerful investigative tool that allowed in vivo quantification of physiologic processes, including myocardial perfusion and metabolism, neuronal and receptor function, and, more recently, molecularly tar-

geted oncologic imaging. Despite its success in research applications, the limited availability of this technology, its increased cost, and the limited data supporting its use and reimbursement have all contributed to the relatively limited clinical acceptance of this imaging technology. Fortunately, there are now clear signs that change is under way. Indeed, the exponential growth in the number of PET/CT systems—attributable primarily to the technology's widely accepted role in clinical oncology—along with the Food and Drug Administration's approval of PET radiopharmaceuticals for cardiac imaging, changes in reimbursement, and the increasing documentation of PET's clinical efficacy have all contributed to help advance its clinical role in cardiovascular medicine.

The emergence of integrated PET/CT technology as the dominant configuration of clinical scanners also holds great promise for cardiac imaging as it provides a potential opportunity to delineate the anatomic extent and physiologic severity of coronary atherosclerosis in a single setting. However, the recent rapid growth of PET/CT is now opening a considerable gap between the most sophisticated users of the technology and those with a more limited knowledge base and fewer training opportunities; this includes cardiologists, as well as nuclear medicine specialists, and radiologists, who frequently lack clinical experience in performing and interpreting these cardiovascular procedures. The objective of this review is to provide trainees and practicing imaging specialists with a practical review of how to perform and interpret myocardial perfusion imaging with PET/CT in the clinical setting.

## RADIOPHARMACEUTICALS

Although several tracers have been used for evaluating myocardial perfusion with PET, the most widely used in clinical practice are <sup>82</sup>Rb and <sup>13</sup>N-ammonia.

### <sup>82</sup>Rb

<sup>82</sup>Rb is a potassium analog that is a generator product with a physical half-life of 76 s and kinetic properties similar to those of <sup>201</sup>Tl (*1*). Because of the distinct advantage of not requiring an on-site cyclotron, <sup>82</sup>Rb is the most widely used radionuclide for assessment of myocardial perfusion with

Received Jan. 16, 2007; revision accepted Mar. 20, 2007.

For correspondence or reprints contact: Marcelo F. Di Carli, MD, Division of Nuclear Medicine/PET, Brigham and Women's Hospital, 75 Francis St., Boston, MA 02115.

E-mail: mdicarli@partners.org

\*NOTE: FOR CE CREDIT, YOU CAN ACCESS THIS ACTIVITY THROUGH THE SNM WEB SITE ([http://www.snm.org/ce\\_online](http://www.snm.org/ce_online)) THROUGH MAY 2008.

Marcelo F. Di Carli reports having an affiliation with GE Healthcare, Bracco Diagnostics, Bristol-Myers Squibb Imaging, Siemens Medical Solutions, and Astellas Pharma US, Inc. No other potential conflict of interest relevant to this article was reported.

COPYRIGHT © 2007 by the Society of Nuclear Medicine, Inc.

PET. Its parent radionuclide is  $^{82}\text{Sr}$ , which has a physical half-life of 26 d. Consequently, the  $^{82}\text{Sr}/^{82}\text{Rb}$  generator is replaced every 4 wk. The generator can be eluted with >90% yield every 10 min. The short physical half-life of  $^{82}\text{Rb}$  and the rapid reconstitution of the generator allow fast sequential perfusion imaging and laboratory throughput, thereby maximizing clinical efficiency.

After intravenous injection,  $^{82}\text{Rb}$  rapidly crosses the capillary membrane (1). Myocardial uptake of  $^{82}\text{Rb}$  requires active transport via the sodium/potassium adenosine triphosphate transporter, which is dependent on coronary blood flow (2). The single-capillary transit extraction fraction of  $^{82}\text{Rb}$  exceeds 50%. However, like other nondiffusible tracers, its net extraction fraction decreases in a nonlinear fashion with increasing myocardial blood flow (2–4).

The maximum kinetic energy of positrons emitted during  $^{82}\text{Rb}$  decay is significantly higher than that of  $^{18}\text{F}$  or  $^{13}\text{N}$ . Consequently, the spatial uncertainty in the location of the decaying nucleus—which depends on the distance traveled by the positrons before their annihilation (positron range)—is greater for  $^{82}\text{Rb}$  (2.6-mm full width at half maximum [FWHM]) than for  $^{18}\text{F}$  (0.2-mm FWHM) or  $^{13}\text{N}$  (0.7-mm FWHM). Although  $^{82}\text{Rb}$  imaging yields excellent image quality with current PET technology, its longer positron range and its short half-life, which requires significant image smoothing to suppress noise, both mitigate somewhat the improved spatial resolution of PET.

### **$^{13}\text{N}$ -Ammonia**

$^{13}\text{N}$ -ammonia is a cyclotron product and has a physical half-life of 9.96 min. After injection,  $^{13}\text{N}$ -ammonia rapidly disappears from the circulation, permitting the acquisition of images of excellent quality. Although the sequestration of  $^{13}\text{N}$ -ammonia in the lungs is usually minimal, it may be increased in patients with depressed left ventricular (LV) systolic function or chronic pulmonary disease and, occasionally, in smokers. This may, in turn, adversely affect the quality of the images. In these cases, it may be necessary to increase the time between injection and image acquisition to optimize the contrast between myocardial and background activity.

In arterial blood,  $^{13}\text{N}$ -ammonia consists of neutral ammonia ( $\text{NH}_3$ ) in equilibrium with its charged ammonium ( $\text{NH}_4$ ) ion. The neutral  $\text{NH}_3$  molecule readily diffuses across plasma and cell membranes, leading to virtually complete extraction from the vascular pool. Inside the myocyte, it reequilibrates with its ammonium form, which is trapped in glutamine via the enzyme glutamine synthase (5,6). Once inside the myocyte,  $^{13}\text{N}$ -ammonia is incorporated into the glutamine pool and becomes metabolically trapped (6). Only a small fraction diffuses back into the intravascular space (6). Its retention by the myocardium has a nonlinear and inverse relationship with blood flow. In healthy humans, the fraction of  $^{13}\text{N}$ -ammonia retained by the myocardium during its first pass is 0.83 when blood flow is 1 mL/min/g, and decreases to 0.60 as flow increases to 3 mL/min/g. As with other nondiffusible tracers,

the net tissue extraction (the product of the retained fraction during first pass and myocardial blood flow) decreases as myocardial blood flow increases. For  $^{13}\text{N}$ -ammonia, the relation between net tissue extraction and blood flow is linear for values of blood flow up to 2.5 mL/min/g. At high flow rates, “metabolic trapping” of  $^{13}\text{N}$ -ammonia becomes the rate-limiting factor affecting tracer retention. This leads to underestimation of blood flow at high flow rates (7). Therefore, to quantify myocardial blood flow using  $^{13}\text{N}$ -ammonia, it becomes necessary to correct for flow-dependent changes in net tissue extraction.

Myocardial retention of  $^{13}\text{N}$ -ammonia is heterogeneous, with retention in the lateral left ventricular (LV) wall being about 10% lower than that of other segments, even in healthy subjects.  $^{13}\text{N}$ -Ammonia images may also be degraded by occasional intense liver activity, which can interfere with the evaluation of the inferior wall. Although the sequestration of  $^{13}\text{N}$ -ammonia in the lungs is usually minimal, it may be increased in patients with depressed LV systolic function or chronic pulmonary disease and, occasionally, in smokers (8). In these cases, it may be necessary to increase the time between injection and image acquisition to optimize the contrast between myocardial and background activity.

$^{13}\text{N}$ -Ammonia allows the acquisition of ungated and gated images of good quality. These studies take full advantage of the superior resolution of PET relative to SPECT, as the half-life of  $^{13}\text{N}$  is sufficiently long and its average positron range is very short. Gated  $^{13}\text{N}$ -ammonia imaging can provide accurate assessments of both regional and global cardiac function (9). However, this imaging agent is not well suited for peak stress gated imaging because of the 3- to 4-min time interval between radiotracer injection and the start of imaging and the relatively long (~20 min) acquisition time.

### **IMAGING PROTOCOLS**

Figure 1 illustrates common protocols used for imaging myocardial perfusion with PET/CT, in which the CT scan is used for attenuation correction.

#### **CT Scans**

Patient positioning is performed with a CT scout image or topogram. This is followed by a low-dose CT scan covering the heart region. It is important to understand that acquisition parameters for CT-based transmission imaging vary with the configuration of the CT scanner (e.g., 8-, 16-, and 64-detector CT) and clinical protocol. However, the general scan settings used in most clinics for CT transmission imaging, independent of the manufacturer, include (a) a slow rotation speed (e.g., 1 s/revolution), combined with a relatively high pitch (e.g., 0.5–0.6:1); (b) a nongated scan; (c) a high tube potential (e.g., 140 kVp) and a low tube current (~10–20 mA); and (d) a CT acquisition obtained during tidal expiration breath-hold or shallow breathing. It is also possible to use a prospectively gated CT scan, in which the x-ray tube is “turned on” only during the end-diastolic phase of the cardiac cycle—typically 75%–80% of the R–R interval, with

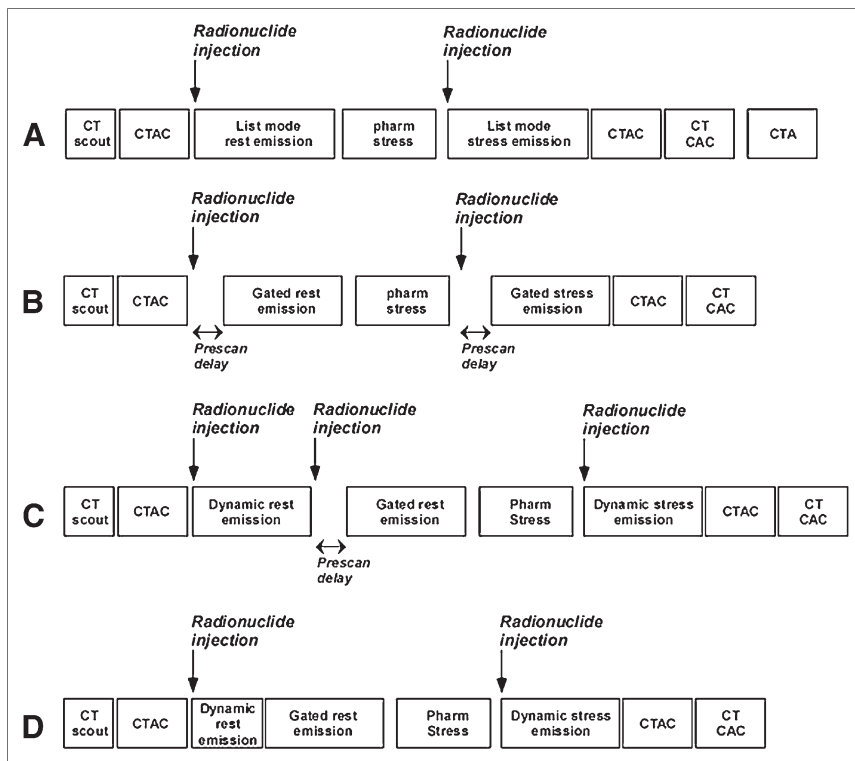


**FIGURE 1.** Protocols for clinical cardiac PET/CT. (A) Hybrid list-mode PET + CTA protocol. (B) Gated PET/CT protocol. (C) Multiframe (dynamic)  $^{82}\text{Rb}$  PET/CT + CAC protocol. (D) Multiframe (dynamic)  $^{13}\text{N}$ -ammonia PET/CT + CAC protocol. CTAC = CT-based attenuation correction (transmission scan); pharm = pharmacologic; CAC = coronary artery calcium scan; CTA = CT angiography.

higher tube current (~250–350 mA) acquired during (preferably) an expiratory breath-hold. This gated CT scan can be used for attenuation correction and for quantification of coronary calcium score. This approach is more challenging because it tends to result in more frequent misalignment between the transmission (breath-hold) and emission (free breathing) images, thereby requiring dedicated software for realignment of the 2 datasets before reconstruction of the PET images. The gated protocol also results in higher radiation dose to the patient compared with the nongated scan (~0.4–0.6 mSv vs. ~1.6 mSv for a 64-slice PET/CT scanner, respectively). It is also generally accepted that the rest and stress emission images should each be corrected with its own dedicated transmission scan due to known changes in cardiac and pulmonary volumes during pharmacologic stress—especially with vasodilators. For the stress images, the best attenuation correction results are usually obtained with postemission transmission imaging (after completion of the stress  $^{82}\text{Rb}$  acquisition). This is due to the fact that, by then, the peak effect of the stress agent used (e.g., adenosine or dipyridamole) has passed, and the patient tends to be more comfortable and, consequently, there is a lower frequency of motion during the acquisition of the CT transmission scan.

In selected patients, it is also possible to obtain a coronary CT angiogram (CTA) immediately after the assessment of myocardial perfusion (Fig. 1A). To perform coronary CTA, a 16-detector or, preferably, a 64-detector CT scanner is required to cover the heart region rapidly enough. In patients undergoing a hybrid study (myocardial perfusion PET + coronary CTA), there is general agree-

ment that the CTA should be performed after the PET scan. This sequence avoids potential interference of intravenous  $\beta$ -blockers used for heart rate control in preparation for the CTA, with the maximal hyperemic or heart rate responses during vasodilator and dobutamine stress, respectively. The CTA imaging protocol has been discussed in detail elsewhere (10). With appropriate training and experience, the integrated protocol can be completed in approximately 30 min.

### Emission Scans

For  $^{82}\text{Rb}$ , approximately the same dose (1.48–2.22 GBq [40–60 mCi]) is injected for the rest and the stress myocardial perfusion studies. For  $^{13}\text{N}$ -ammonia, the general trend is to use a lower activity for the rest images (~0.37 GBq [~10 mCi]) and a higher activity for the stress images (~1.11 GBq [~30 mCi]). Ideally, the doses of the radiotracers should also be adjusted according to the size of the patient and, importantly, the type of PET data acquisition (i.e., 2-dimensional vs. 3-dimensional [3D] mode). The low-dose/high-dose protocol is faster (than the same dose protocols for rest and stress) as it does not require waiting for decay of  $^{13}\text{N}$  to background levels before a second dose can be administered. However, large patients may require relatively large doses for both the rest and the stress studies (analogous to the 2-d  $^{99\text{m}}\text{Tc}$  SPECT protocol). Some laboratories perform stress imaging first, as a normal scan may avoid the need for rest imaging. The downside of “stress-only” imaging is that there will be no opportunity to obtain rest and stress LV ejection fraction (LVEF) or myocardial blood flow and coronary vasodilator reserve, thereby limiting the ability to identify patients with

extensive coronary artery disease (CAD) and “balanced” ischemia.

There are several ways in which the emission images can be acquired. These include:

- **ECG Gated Imaging.** This is the most common clinical approach. Imaging begins 90–120 s after  $^{82}\text{Rb}$  injection, or 3–5 min after  $^{13}\text{N}$ -ammonia injection, to allow for clearance of radioactivity from the lungs and blood pool; the scan duration is approximately 5 or 20 min for  $^{82}\text{Rb}$  or  $^{13}\text{N}$ -ammonia, respectively (Fig. 1B). The number of gated frames is usually set to 8 or 16, with rejection of ectopic beats outside the acceptance window.
- **Multiframe or Dynamic Imaging.** Imaging begins with the bolus (short infusion) of  $^{82}\text{Rb}$  or  $^{13}\text{N}$ -ammonia and continues for 7–8 min or 20 min, respectively (Fig. 1C). The advantage of this approach is that it allows quantification of myocardial blood flow (in mL/min/g)—for example, by fitting regional tissue and blood time–activity curves to a suitable kinetic model. However, its main disadvantage is that one needs to perform a separate radionuclide injection to obtain ECG-gated images from which to assess cardiac function, especially when using  $^{82}\text{Rb}$ . Using  $^{13}\text{N}$ -ammonia, one can acquire a short multiframe or dynamic scan (4 min) that can be followed with a separate ~15-min ECG-gated scan to assess myocardial perfusion and LVEF, without the need for an additional radionuclide injection because of its longer physical half-life (~10 min) (Fig. 1D). To measure the LV blood time–activity curve noninvasively, one must acquire many dynamic PET image frames while the tracer bolus passes through the right ventricle (RV), the lungs, and the LV. During this interval, it is common for a relatively large amount of activity (~0.74–1.11 GBq [~20–30 mCi]) to be located entirely within the PET scanner’s axial field of view. Because of possible counting-rate limitations under such conditions—particularly in the 3D (septalless) scan mode—great care must be taken to ensure the accuracy of the PET system’s corrections for random and scatter coincidences as well as dead time. Although quantitative inaccuracies seen at high counting rates may be mitigated by injecting less activity, this could yield too much image noise in the later (tissue) phase of the dynamic study, so a careful compromise needs to be determined for each given PET system and scan mode.
- **List-Mode Imaging.** This is the ideal approach because a single injection and data acquisition allows multiple image reconstructions (i.e., summed, ECG gated, and multiframe or dynamic) for a comprehensive physiologic examination of the heart. With this approach, image acquisition commences with the bolus injection of the radionuclide and continues for 7–8 min or 20 min for  $^{82}\text{Rb}$  and  $^{13}\text{N}$ -ammonia, respectively (Fig. 1A). List-mode imaging requires significant computer

power to perform the multiple reconstructions, especially for the 3D image acquisition mode.

Stress testing can be performed with pharmacologic means (e.g., adenosine, dipyridamole, or dobutamine)—most common—or with exercise (11). The latter is easier with  $^{13}\text{N}$ -ammonia (half-life of ~10 min) than with  $^{82}\text{Rb}$  (half-life of 76 s).

#### QUALITY ASSURANCE FOR CARDIAC PET/CT

Performing good-quality cardiac PET/CT is technically demanding and, thus, familiarity with key quality control steps is crucial to optimize clinical results. These quality control measures include routine inspection of the transmission and emission data and the transmission-emission alignment. A description of routine maintenance, calibration, and quality control of the PET/CT scanner is beyond the scope of this review; however, the reader is encouraged to review excellent recent discussions on the subject (12,13).

#### Count Density

The level of statistical noise in the emission and transmission images should be checked to see whether enough counts have been acquired. This is crucial with  $^{82}\text{Rb}$  imaging because of the short half-life of the isotope. Although the image quality of CT transmission images may be suboptimal in heavy patients, this does not appear to compromise the quality of the attenuation correction because the attenuation map is integrated along the PET lines of response to obtain attenuation-correction factors. Also, of course, many more transmitted photons are used for CT, even with a low (10–20 mA) tube current, than for a transmission-source (e.g.,  $^{68}\text{Ge}$ ) scan on a conventional PET system. Hence, it is not necessary to increase the CT dose in heavy patients. The most common sources of count-poor emission studies include large patient size, inadequate radionuclide dose or delivery (e.g., problems with intravenous access), or inadequate scan duration.

#### Ratio of Heart to Blood-Pool Counts

Acquisition of emission images before complete clearance of radiotracer from the blood pool may potentially degrade image quality. The optimal prescan delay for acquisition of  $^{13}\text{N}$ -ammonia images is ~3 min and for  $^{82}\text{Rb}$  images is ~90 s in healthy subjects. The most common factors that prolong circulation time of the radionuclide include severe LV systolic dysfunction (LVEF < 30%, either chronic or acute because of severe ischemia during stress), RV systolic dysfunction, and primary lung disease. In those clinical settings, increased prescan delay is usually required to improve image quality (14). As discussed earlier, multiframe (i.e., dynamic) or list-mode imaging protocols are very helpful, as assumptions with regard to prescan delay are not required.

#### Transmission–Emission Misalignment

Misregistration of transmission and emission images can result from respiratory or patient motion, and it can degrade image quality and lead to inaccurate clinical results (15–17).

Because of the circular arrays of scintillation detectors in PET/CT cameras, patient movement during imaging affects all projections and can be very difficult to detect by direct inspection of the rotating projections, as assessed with SPECT. Because transmission and emission imaging is sequential, patient or respiratory (e.g., deep inspiration) motion during the emission images will most likely lead to transmission–emission misalignment and potential attenuation-correction artifacts (Fig. 2). The extent and direction of this misalignment will determine whether artifacts will be apparent in the attenuation-corrected images. Most commercial PET/CT systems now include software tools to correct for transmission–emission misalignments. This tool allows correction of the sinograms before tomographic reconstruction and rereconstruction with the correct attenuation map.

### Image Reconstruction Artifacts

Artifacts resulting from filtered backprojection reconstruction algorithms, image truncation, and CT transmission artifacts, such as beam hardening, may be observed with cardiac PET/CT. As seen in SPECT myocardial perfusion imaging, excessive subdiaphragmatic activity from high counts in the liver or bowel may result in decreased counts in the adjacent inferior LV wall when filtered backprojection is used for image reconstruction. This artifact may be

particularly problematic if seen only on the stress images because it may cause an apparent reversible perfusion defect. Fortunately, artifacts from filtered backprojection are not common with PET as iterative methods are generally used for image reconstruction. Streak artifacts may be seen in large patients with arms-down imaging (a result of beam hardening from the large bones) or with metal implants in the field of view. In PET/CT systems that allow transmission imaging with an external radioactive source, this approach may obviate the limitations of CT-based transmission imaging. Preliminary evidence suggests that a segmented reconstruction algorithm for the CT scan may help overcome artifacts from metallic implants (18). Residual radiotracer activity in the intravenous line within the field of view may be an additional source of image reconstruction artifacts that can be minimized by flushing the intravenous tubing.

### DIAGNOSTIC ACCURACY

Table 1 summarizes the published studies documenting the diagnostic accuracy of myocardial perfusion PET for detecting obstructive CAD. The average weighted sensitivity for detecting at least one coronary artery with >50% stenosis is 90% (range, 83%–100%), whereas the average specificity is 89% (range, 73%–100%). The corresponding average positive and negative predictive values (PPV and

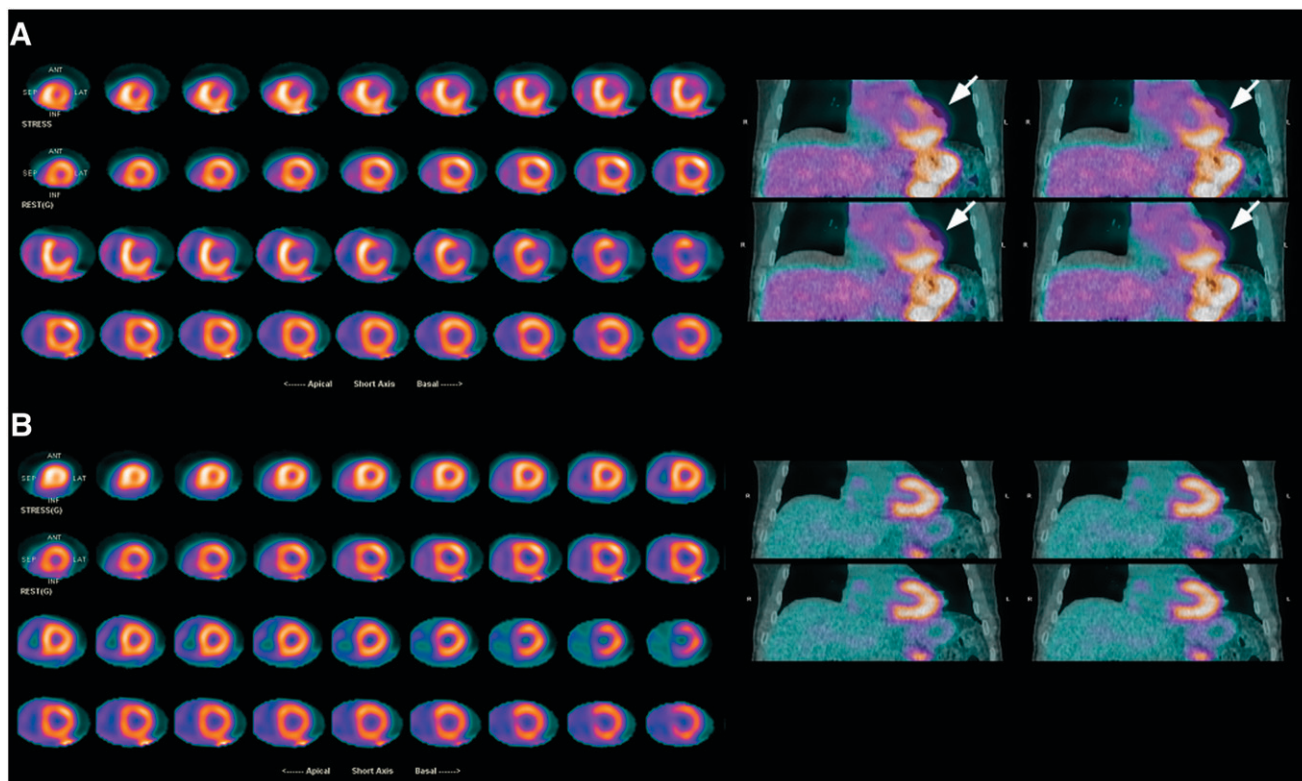


**FIGURE 2.** Transmission–emission misalignment. (A) Misaligned CT transmission and  $^{82}\text{Rb}$  images (right) and resulting anterolateral perfusion defect on stress–rest  $^{82}\text{Rb}$  PET (left). Perfusion defect results from applying incorrect attenuation coefficients during tomographic reconstruction to area of LV myocardium overlying lung field on CT transmission scan (arrows). (B) Correction of emission–transmission misalignment (right) and resulting normal perfusion study.

**TABLE 1**  
Summary of Published Literature with Regard to Diagnostic Accuracy of PET

Reference	No. of patients	Women	Prior CAD	PET radiotracer	Sensitivity	Specificity	PPV	NPV	Accuracy
Sampson et al. (22)*	102	0.42	0	<sup>82</sup> Rb	0.93	0.83	0.80	0.94	0.87
Bateman et al. (21)	112	0.46	0.25	<sup>82</sup> Rb	0.87	0.93	0.95	0.81	0.89
Marwick et al. (23)	74	0.19	0.49	<sup>82</sup> Rb	0.90	1	1	0.36	0.91
Grover-McKay et al. (24)	31	0.01	0.13	<sup>82</sup> Rb	1	0.73	0.80	1	0.87
Stewart et al. (20)	81	0.36	0.42	<sup>82</sup> Rb	0.83	0.86	0.94	0.64	0.84
Go et al. (19)	202	NR	0.47	<sup>82</sup> Rb	0.93	78	0.93	0.80	0.90
Demer et al. (25)	193	0.26	0.34	<sup>82</sup> Rb / <sup>13</sup> N-ammonia	83	0.95	0.98	0.60	0.85
Tamaki et al. (26)	51	NR	0.75	<sup>13</sup> N-ammonia	0.98	1	1	0.75	0.98
Gould et al. (27)	31	NR	NR	<sup>82</sup> Rb / <sup>13</sup> N-ammonia	0.95	1	1	0.90	0.97
Weighted summary	877	0.29	0.35		0.90	0.89	0.94	0.73	0.90

\*Study using PET/CT (in which CT was used for attenuation correction only).

PPV = positive predictive value; NPV = negative predictive value; NR = not reported.

(Reprinted with permission of (28).)

NPV, respectively) are 94% (range, 80%–100%) and 73% (range, 36%–100%), respectively, and the overall diagnostic accuracy is 90% (range, 84%–98%). Most of the available data has been obtained with dedicated PET cameras, rather than with PET/CT systems. However, in a recent study using PET/CT (in which the CT was used only for attenuation correction), Sampson et al. (22) reported a sensitivity of 93%, a specificity of 83%, with a normalcy rate of 100%. In this study of patients without known prior CAD, the PPV and NPV of PET/CT were 80% and 94%, respectively, with an overall accuracy of 87%. These results were applicable to men and women as well as obese and nonobese individuals.

#### Comparative Studies of PET Versus SPECT

Three studies have performed a direct comparison of the diagnostic accuracy of <sup>82</sup>Rb myocardial perfusion PET and <sup>201</sup>Tl or <sup>99m</sup>Tc SPECT in the same or matched patient populations. Go et al. compared PET and SPECT in 202 patients (19). Their results showed a higher sensitivity with PET than with SPECT (93% vs. 76%, respectively), without significant changes in specificity (78% vs. 80%, respectively). In another study, Stewart et al. compared PET and SPECT in 81 patients (20). They observed a higher specificity for PET than with SPECT (83% vs. 53%, respectively), without significant differences in sensitivity (86% vs. 84%, respectively). Diagnostic accuracy was higher with PET than with SPECT (89% vs. 78%, respectively). The differences between these 2 studies are likely to be attributable to patient selection, resulting in differences in prescan likelihood of CAD.

More recently, Bateman et al. compared <sup>82</sup>Rb PET and <sup>99m</sup>Tc-sestamibi SPECT in 2 matched patient cohorts undergoing clinically indicated pharmacologic-stress perfusion imaging using contemporary technology for both SPECT and PET (21). The overall diagnostic accuracy

using either a 50% or a 70% angiographic threshold was higher for PET than for SPECT (87% vs. 71% with a 50% threshold, and 89% vs. 79% with a 70% threshold). Differences in diagnostic accuracy reflected primarily the increased specificity (with a marginal advantage in sensitivity) of PET vs. SPECT and applied to both men and women and to obese and nonobese individuals.

#### EVALUATING MULTIVESSEL CAD

Although the relative assessment of myocardial perfusion with PET remains a sensitive means for diagnosing or ruling out the presence of obstructive CAD in individual patients, PET (like SPECT) often uncovers only the coronary territory supplied by the most severe stenoses. This is because the coronary vasodilator reserve is often abnormal in patients with CAD—even in territories supplied by noncritical angiographic stenoses (29,30)—thereby reducing the heterogeneity of flow between “normal” and “abnormal” zones and limiting the ability to delineate the presence of multivessel CAD.

An advantage of ECG-gated PET is its distinct ability to assess LV function at rest and during peak stress (as opposed to poststress with gated SPECT). Recent data from our laboratory suggest that in healthy subjects, LVEF increases during peak vasodilator stress (31). In the presence of CAD, however, changes in LVEF (from baseline to peak stress) are inversely related to the magnitude of perfusion abnormalities during stress (reflecting myocardium at risk) (Fig. 3). In patients with 3-vessel CAD or left main CAD, LVEF during peak stress decreases even in the absence of apparent perfusion abnormalities (Figs. 4 and 5). In contrast, patients without significant CAD or with 1-vessel disease show a normal increase in LVEF. Consequently, the NPV of a delta increase in LVEF (from rest to peak stress) of  $\geq 5\%$  to exclude the presence 3-vessel or left main CAD is 97% (31).

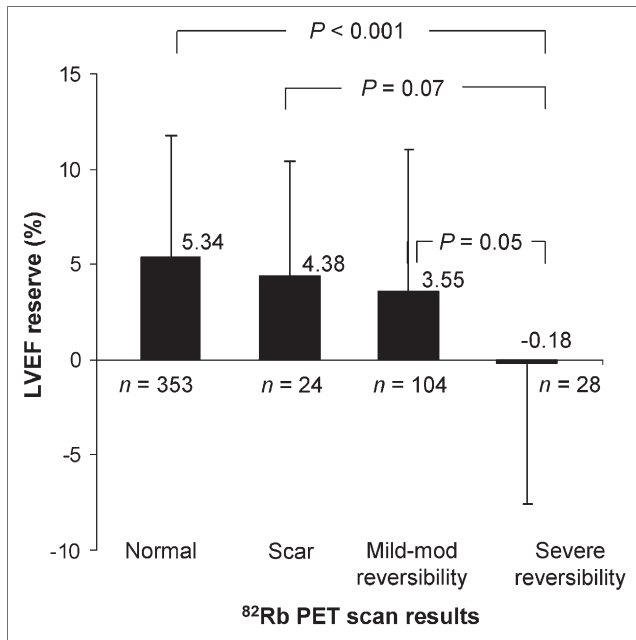


**FIGURE 3.** Bar graph demonstrates relationship between magnitude of stress-induced perfusion abnormalities and delta change in LVEF (from baseline to peak stress) (31). mod = moderate.

Alternatively, PET measurements of myocardial blood flow (in mL/min/g of myocardium) and coronary vasodilator reserve may also help overcome the limitations of relative perfusion assessments with PET to uncover the presence of multivessel CAD. There is consistent experimental (32) and clinical (33–35) evidence supporting the notion that noninvasive measurements of myocardial blood

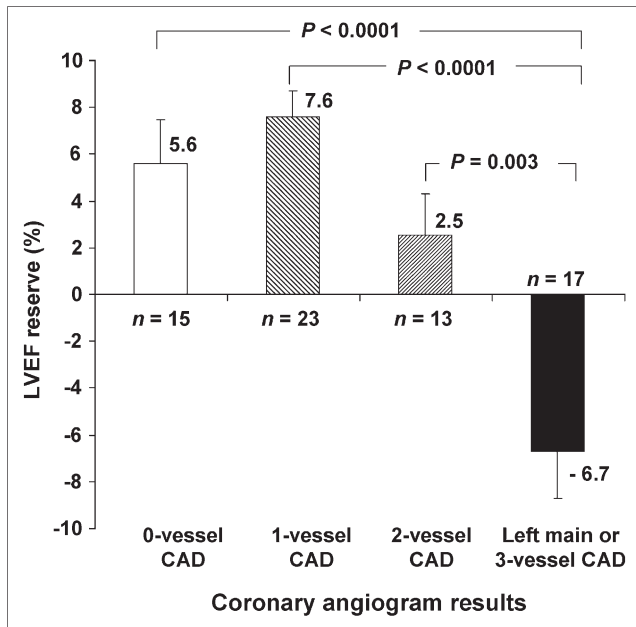


**FIGURE 4.** Bar graph demonstrates relationship between extent of angiographic CAD (>70% stenosis) and delta change in LVEF (31).

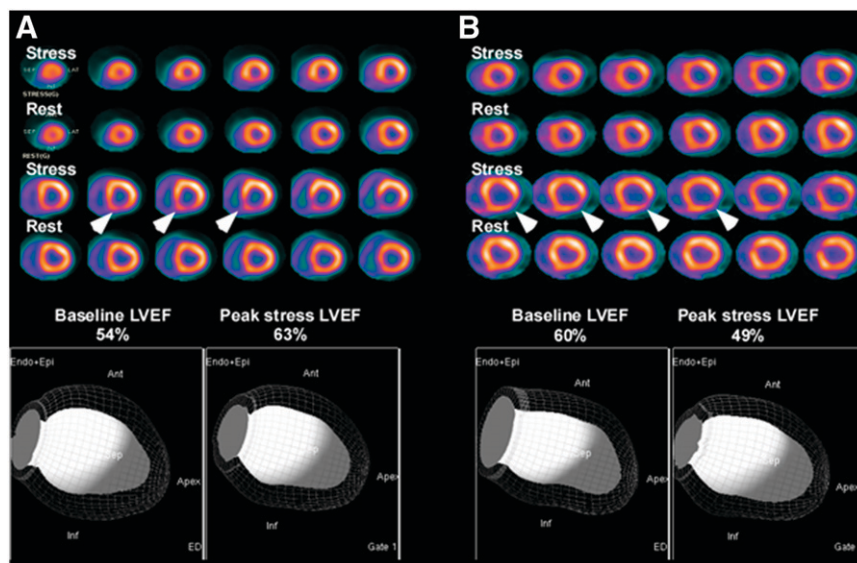
flow (in mL/min/g of tissue) and coronary vasodilator reserve (the ratio between peak and rest myocardial blood flow) by PET are inversely and nonlinearly related to stenosis severity. There is growing, consistent evidence that these quantitative estimates of coronary hemodynamics by PET allow better definition of the extent of anatomic CAD (30,36). For example, Yoshinaga et al. (30) showed good agreement between SPECT defects and PET measures of coronary vasodilator reserve in only 16 of 58 (28%) territories supplied by vessels with stenoses > 50% as assessed by quantitative angiography. The remaining 42 of 58 (72%) territories with angiographic stenoses showed no regional perfusion defects by SPECT but an abnormal vasodilator reserve by PET. Likewise, Parkash et al. (36) found that in patients with 3-vessel CAD, perfusion defect sizes were significantly larger using quantitative myocardial blood flow estimates as compared with the traditional circumferential profile method ( $44\% \pm 18\%$  vs.  $69\% \pm 24\%$ ).

PET quantification of myocardial blood flow is well validated using  $^{13}\text{N}$ -ammonia (37–39). Quantitative approaches with  $^{82}\text{Rb}$  are more challenging because of its very short physical half-life and, thus, its decreased image signal-to-noise ratio, leading to noisy and inconsistent time–activity curves that can affect the accuracy of myocardial perfusion estimates. However, the use of noise-reduction methods improves the accuracy and precision of measurements of myocardial blood flow (40,41), which conceptually supports the notion that it is possible to quantify myocardial perfusion using  $^{82}\text{Rb}$ . Our group has reported improved reproducibility of quantitative myocardial perfusion measurements with  $^{82}\text{Rb}$  by using factor analysis to better separate the tissue and arterial blood time–activity curves (42,43) (Fig. 6). Validation studies in animals and humans are currently under way.

## RISK STRATIFICATION

With the increased clinical use of PET and PET/CT in stress myocardial perfusion imaging, data documenting its incremental prognostic value are beginning to emerge. The prognostic value of dipyridamole stress  $^{82}\text{Rb}$  PET was recently investigated in 367 patients with follow-up for  $3.1 \pm 0.9$  y (44). As has been previously described with SPECT, increasing extent and severity of perfusion defects with stress PET was associated with increasing frequency of adverse events. Importantly, the hard event rate (i.e., myocardial infarction or cardiac death) in patients with normal stress PET was 0.4%/y. However, this study—the largest PET prognosis study to date—was limited by the occurrence of only 17 hard events. Preliminary data from our laboratory in 1,602 consecutive patients undergoing rest–stress  $^{82}\text{Rb}$  myocardial perfusion PET/CT also suggest that this technique provides incremental value to clinical variables in predicting overall survival (45). Unlike previous studies, this study was adequately powered by the

**FIGURE 5.** Gated rest–stress  $^{82}\text{Rb}$  myocardial perfusion PET images illustrate added value of LV function over perfusion information. (A) Normal rise in LVEF from rest to peak stress (bottom) in patient with angiographic single-vessel CAD, showing single perfusion defect in inferior wall on PET images (arrowheads). (B) Abnormal reduction in LVEF from rest to peak stress in patient with angiographic multivessel CAD, also showing single perfusion defect in inferolateral wall on PET images (arrowheads). Ant = anterior; Inf = inferior. (Reprinted with permission of (28).)



occurrence of 113 deaths (7% of the study cohort) during a median follow-up period of 511 d. In keeping with previous studies, increases in the extent and severity of stress perfusion defects translated into proportional increases in

predicted mortality. In addition, preliminary data from our laboratory in 1,274 consecutive patients also confirm the incremental prognostic value of LVEF over stress perfusion imaging (46). As expected, this analysis showed that the mortality hazard was inversely related to the LVEF. Importantly, myocardial perfusion imaging added incremental value to LVEF (at any LVEF, a higher summed stress score had greater risk) and LVEF added incremental value to myocardial perfusion imaging (i.e., at any summed stress score, a lower LVEF had greater risk).

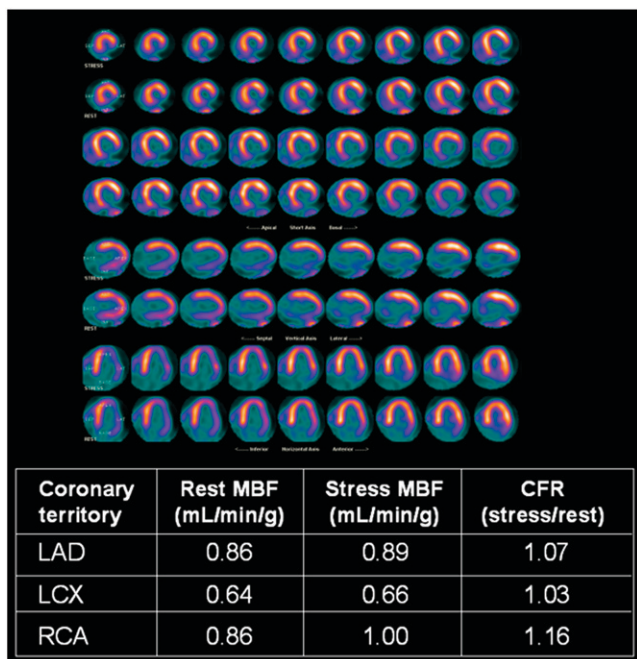


**FIGURE 6.** (Top) Stress–rest  $^{82}\text{Rb}$  PET scan demonstrates a large and severe perfusion defect throughout inferior and inferolateral LV walls, which was fixed. (Bottom) Results of quantitative assessment of myocardial blood flow from  $^{82}\text{Rb}$  PET approach developed at Brigham and Women’s Hospital. Data demonstrate severely impaired dipyridamole-stimulated myocardial blood flow (MBF), resulting in a markedly reduced coronary flow reserve (CFR). Coronary angiography demonstrated total occlusion of right and left circumflex coronary arteries and severe stenosis in mid left anterior descending artery. LAD = left anterior descending coronary artery; LCX = left circumflex coronary artery; RCA = right coronary artery.

## INTEGRATED ASSESSMENT OF MYOCARDIAL PERFUSION AND CORONARY ANGIOGRAPHY

The integration of PET and multidetector CT scanners has interesting potential in cardiology. This technology enables detection and quantification of the burden of calcified and noncalcified plaques, quantification of vascular reactivity and endothelial health, identification of flow-limiting coronary stenoses, and, potentially, identification of high-risk plaques (through fusion of anatomy and biology with molecularly targeted PET) in the coronary and other arterial beds in the same setting.

### Assessing Atherosclerosis Burden

Integrated PET/CT offers an opportunity to assess the presence and magnitude of subclinical atherosclerotic disease burden and to measure myocardial blood flow (in mL/min/g of myocardium) as a marker of endothelial health and atherosclerotic disease activity. Recent evidence comparing the results of cardiac CT and myocardial perfusion imaging suggest that a significant proportion of patients with normal myocardial perfusion studies have evidence of subclinical atherosclerosis (sometimes extensive) by CTA (47). This finding is not unexpected, as the main advantage of the myocardial perfusion imaging method is its ability to identify flow-limiting stenoses. Although it is premature to

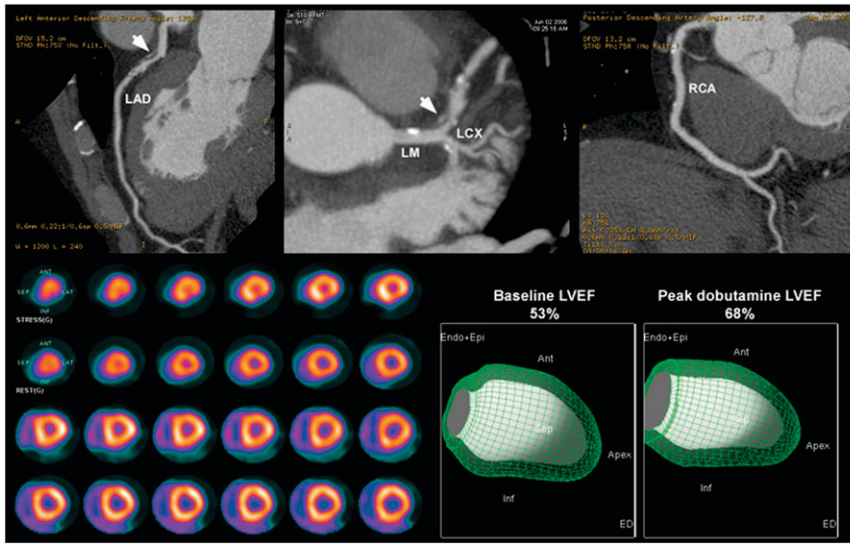


**FIGURE 7.** Integrated PET/CTA study. CTA images demonstrate noncalcified plaque (arrow) in proximal LAD with 50%–70% stenosis. However, rest and peak dobutamine stress myocardial perfusion PET study (bottom left panel) demonstrates only minimal inferoapical ischemia. In addition, LVEF was normal at rest and demonstrated a normal rise during peak dobutamine stress. LAD = left anterior descending coronary artery; LCX = left circumflex coronary artery; LM = left main coronary artery; RCA = right coronary artery; Ant = anterior; Inf = inferior. (Reprinted with permission of (28).)

predict the clinical significance of this observation, it provides intriguing evidence for future investigations of the potential complementary role of CTA and perfusion imaging for individualizing risk stratification and patient management. Whereas myocardial perfusion imaging will likely continue to define the need for revascularization, the objective assessment of atherosclerotic burden (both calcified and noncalcified plaques) by CTA might be able to

play a role in individualizing the intensity and goals of medical therapy.

### Guiding Management of CAD

Because not all coronary stenoses detected by CTA are flow limiting, the stress myocardial perfusion PET data complement the CT anatomic information by providing instant readings about the clinical significance (i.e., ischemic burden) of such stenoses (Fig. 7). Recent data from multiple laboratories using either sequential imaging (CTA followed by SPECT) (48,49) or hybrid imaging (SPECT/CT or PET/CT) (47,50) suggest that the PPV of CTA for identifying coronary stenoses producing objective evidence of stress-induced ischemia is suboptimal (Fig. 8). This is consistent with the well-described limitations of anatomic measures of CAD for delineating the physiologic implications of stenoses (51). First, the percent diameter stenosis is only a modest descriptor of coronary resistance as it does not incorporate other lesion characteristics (e.g., length, shape, eccentricity) or stenoses in series that may greatly

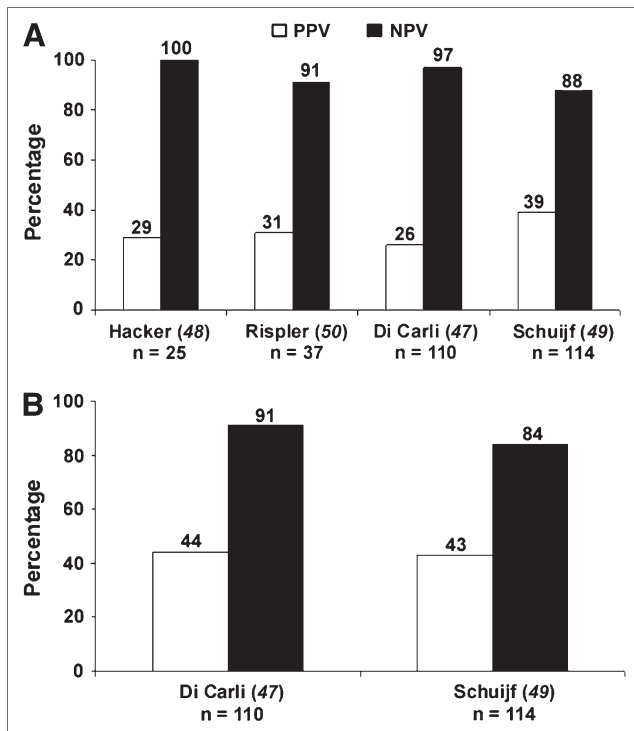


**FIGURE 8.** Frequency of inducible ischemia by myocardial perfusion imaging in territories supplied by stenosis > 50% on CT coronary angiography. (A) Per-vessel analysis. (B) Per-patient analysis. (Reprinted with permission of (28).)

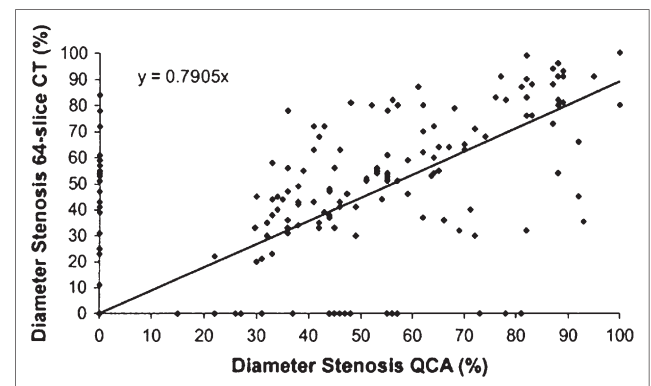
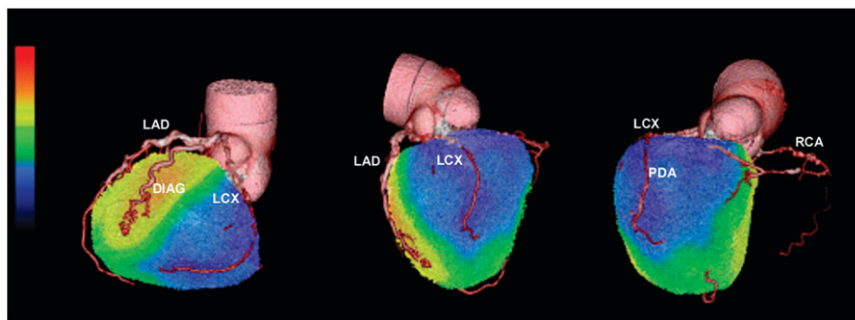


**FIGURE 9.** Correlation between quantitative coronary angiography (QCA) and 64-slice CTA measurements of diameter stenosis in diseased coronary artery segments. Pearson correlation coefficient  $r = 0.54$ . (Reprinted with permission of (52).)

**FIGURE 10.** Fused 3D reconstructions of coronary CTA and stress  $^{82}\text{Rb}$  myocardial perfusion study obtained in same setting, assessed through integrated PET/CTA. CTA demonstrated 3-vessel CAD. Fused CTA stress myocardial perfusion images demonstrate large area of severe stress-induced perfusion abnormality (deep blue color) only in territory of dominant LCX coronary artery. LAD = left anterior descending coronary artery; DIAG = diagonal artery; LCX = left circumflex coronary artery; RCA = right coronary artery; PDA = posterior descending artery.



affect the impedance to blood flow. Second, vasomotor tone and coronary collateral flow, both of which are known to affect myocardial perfusion, are not assessed by simple measures of stenosis severity. Finally, as described earlier, CTA is limited in its ability to accurately define the severity of stenosis (a surrogate of physiologic significance) (Fig. 9). In contrast, myocardial perfusion imaging provides a simple and accurate integrated measure of the effect of all of these parameters on coronary resistance and tissue perfusion, thereby optimizing selection of patients who may ultimately benefit from revascularization. This finding, if confirmed in larger studies, would suggest that additional noninvasive testing would be required after CTA before consideration for invasive catheterization. Furthermore, the use of CTA alone in patients with atherosclerosis without myocardial perfusion imaging would potentially result in an enormous increase in the costs of care and resource use due to unnecessary downstream catheterization and revascularization procedures (53).

In addition, image fusion of the stress perfusion PET data with the coronary CT information can also help identify the culprit stenosis in a patient presenting with chest pain and help guide targeted coronary interventions (Fig. 10).

At the moment, there is insufficient data to guide the optimal, efficient use of hybrid imaging in the patient with known or suspected CAD. The complementary nature of stress PET and CTA make a hybrid approach appealing as a potential “1-stop shop” for CAD patients, as the reported data will include rest and peak stress LV perfusion, rest and peak stress LV size and function, coronary anatomy, and atherosclerosis assessment. In the near future, this is also likely to include plaque morphology, coronary vasodilator reserve, and image fusion images to assess culprit lesions. A pivotal question for future research is whether the hybrid approach is a cost-effective one or whether the CTA and PET data are better acquired in a staged approach with 1 of the 2 tests serving as a screen for the other. It is likely that software will permit the same image fusion to be achieved whether the data are acquired on a hybrid system or on 2 separate PET and CTA systems. It seems possible that, depending on a patient’s pretest likelihood of CAD and underlying risk, a lower-likelihood patient may be optimally imaged with a CTA-first approach, whereas a higher-

likelihood patient may benefit more from a PET-first approach, and still other patient subsets may require a hybrid approach. Ongoing clinical trials will define these cohorts (54).

## CONCLUSION

Innovation in noninvasive cardiovascular imaging is rapidly advancing our ability to image in great detail the structure and function of the heart and vasculature. By providing concurrent quantitative information about myocardial perfusion and metabolism with coronary and cardiac anatomy, PET/CT offers the opportunity for a comprehensive noninvasive evaluation of the consequences of atherosclerosis in the coronary arteries and the myocardium. This integrated platform for assessing anatomy and biology offers a great potential for translating advances in molecularly targeted imaging into humans. The goals of future investigation will be to refine these technologies, address the issue of cost-effectiveness, and validate a range of clinical applications in large-scale clinical trials.

## REFERENCES

- Schelbert HR. Evaluation of myocardial blood flow in cardiac disease. In: Skorton DJ, Schelbert HR, Wolf GL, Brundage BH, eds. *Cardiac Imaging: A Companion to Braunwald’s Heart Disease*. Philadelphia, PA: W.B. Saunders; 1991:1093–1112.
- Selwyn AP, Allan RM, L’Abbate A, et al. Relation between regional myocardial uptake of rubidium-82 and perfusion: absolute reduction of cation uptake in ischemia. *Am J Cardiol*. 1982;50:112–121.
- Mullani NA, Goldstein RA, Gould KL, et al. Myocardial perfusion with rubidium-82. I. Measurement of extraction fraction and flow with external detectors. *J Nucl Med*. 1983;24:898–906.
- Goldstein RA, Mullani NA, Marani SK, Fisher DJ, Gould KL, O’Brien HA Jr. Myocardial perfusion with rubidium-82. II. Effects of metabolic and pharmacologic interventions. *J Nucl Med*. 1983;24:907–915.
- Schelbert HR, Phelps ME, Hoffman EJ, Huang SC, Selin CE, Kuhl DE. Regional myocardial perfusion assessed with N-13 labeled ammonia and positron emission computerized axial tomography. *Am J Cardiol*. 1979;43:209–218.
- Schelbert HR, Phelps ME, Huang SC, et al. N-13 ammonia as an indicator of myocardial blood flow. *Circulation*. 1981;63:1259–1272.
- Hutchins GD, Schwaiger M, Rosenspire KC, Krivokapich J, Schelbert H, Kuhl DE. Noninvasive quantification of regional blood flow in the human heart using N-13 ammonia and dynamic positron emission tomographic imaging. *J Am Coll Cardiol*. 1990;15:1032–1042.
- Tamaki N, Ruddy TD, Dekamp R. Myocardial perfusion. In: Wahl RL, Buchanan JW, eds. *Principles and Practice of Positron Emission Tomography*. Philadelphia, PA: Lippincott, Williams & Wilkins; 2002:320–333.

9. Hickey KT, Sciacca RR, Bokhari S, et al. Assessment of cardiac wall motion and ejection fraction with gated PET using N-13 ammonia. *Clin Nucl Med*. 2004; 29:243–248.
10. Hoffmann U, Ferencik M, Cury RC, Pena AJ. Coronary CT angiography. *J Nucl Med*. 2006;47:797–806.
11. Chow BJ, Beanlands RS, Lee A, et al. Treadmill exercise produces larger perfusion defects than dipyridamole stress N-13 ammonia positron emission tomography. *J Am Coll Cardiol*. 2006;47:411–416.
12. DiFilippo FP. Instrumentation and principles of imaging: PET. In: Di Carli MF, Lipton MJ, eds. *Cardiac PET and PET/CT Imaging*. New York, NY: Springer-Verlag. In press.
13. Townsend DW, Besozzi MC, Carney JPC. Integrated PET/CT. In: Di Carli MF, Lipton MJ, eds. *Cardiac PET and PET/CT Imaging*. New York, NY: Springer-Verlag. In press.
14. Bacharach SL, Bax JJ, Case J, et al. PET myocardial glucose metabolism and perfusion imaging. Part 1. Guidelines for data acquisition and patient preparation. *J Nucl Cardiol*. 2003;10:543–556.
15. Bettinardi V, Gilardi MC, Lucignani G, et al. A procedure for patient repositioning and compensation for misalignment between transmission and emission data in PET heart studies. *J Nucl Med*. 1993;34:137–142.
16. Lohgin C, Sdringola S, Gould KL. Common artifacts in PET myocardial perfusion images due to attenuation-emission misregistration: clinical significance, causes, and solutions. *J Nucl Med*. 2004;45:1029–1039.
17. McCord ME, Bacharach SL, Bonow RO, Dilsizian V, Cuocolo A, Freedman N. Misalignment between PET transmission and emission scans: its effect on myocardial imaging. *J Nucl Med*. 1992;33:1209–1214; discussion 1214–1215.
18. Mirzaei S, Guerchaff M, Bonnier C, Knoll P, Doat M, Braeutigam P. Use of segmented CT transmission map to avoid metal artifacts in PET images by a PET-CT device [abstract]. *BMC Nucl Med*. 2005;5(1):3.
19. Go RT, Marwick TH, MacIntyre WJ, et al. A prospective comparison of rubidium-82 PET and thallium-201 SPECT myocardial perfusion imaging utilizing a single dipyridamole stress in the diagnosis of coronary artery disease [see comments]. *J Nucl Med*. 1990;31:1899–1905.
20. Stewart RE, Schwaiger M, Molina E, et al. Comparison of rubidium-82 positron emission tomography and thallium-201 SPECT imaging for detection of coronary artery disease. *Am J Cardiol*. 1991;67:1303–1310.
21. Bateman TM, Heller GV, McGhie AI, et al. Diagnostic accuracy of rest/stress ECG-gated Rb-82 myocardial perfusion PET: comparison with ECG-gated Tc-99m sestamibi SPECT. *J Nucl Cardiol*. 2006;13:24–33.
22. Sampson UK, Limaye A, Dorbala S, et al. Diagnostic accuracy of rubidium-82 myocardial perfusion imaging with hybrid positron emission tomography/computed tomography (PET-CT) in the detection of coronary artery disease. *J Am Coll Cardiol*. 2007;49:1052–1058.
23. Marwick TH, Nemeck JJ, Stewart WJ, Salcedo EE. Diagnosis of coronary artery disease using exercise echocardiography and positron emission tomography: comparison and analysis of discrepant results. *J Am Soc Echocardiogr*. 1992;5: 231–238.
24. Grover-McKay M, Ratib O, Schwaiger M, et al. Detection of coronary artery disease with positron emission tomography and rubidium 82. *Am Heart J*. 1992;123:646–652.
25. Demer LL, Gould KL, Goldstein RA, et al. Assessment of coronary artery disease severity by positron emission tomography: comparison with quantitative arteriography in 193 patients. *Circulation*. 1989;79:825–835.
26. Tamaki N, Yonekura Y, Senda M, et al. Value and limitation of stress thallium-201 single photon emission computed tomography: comparison with nitrogen-13 ammonia positron tomography. *J Nucl Med*. 1988;29:1181–1188.
27. Gould KL, Goldstein RA, Mullani NA, et al. Noninvasive assessment of coronary stenoses by myocardial perfusion imaging during pharmacologic coronary vasodilation. VIII. Clinical feasibility of positron cardiac imaging without a cyclotron using generator-produced rubidium-82. *J Am Coll Cardiol*. 1986;7:775–789.
28. Di Carli MF, Hachamovitch R. New technology for noninvasive imaging of coronary artery disease. *Circulation*. 2007;115:1464–1480.
29. Uren NG, Crake T, Lefroy DC, de Silva R, Davies GJ, Maseri A. Reduced coronary vasodilator function in infarcted and normal myocardium after myocardial infarction [see comments]. *N Engl J Med*. 1994;331:222–227.
30. Yoshinaga K, Katoh C, Noriyasu K, et al. Reduction of coronary flow reserve in areas with and without ischemia on stress perfusion imaging in patients with coronary artery disease: a study using oxygen 15-labeled water PET. *J Nucl Cardiol*. 2003;10:275–283.
31. Dorbala S, Vangala D, Sampson U, Limaye A, Kwong R, Di Carli MF. Value of left ventricular ejection fraction reserve in evaluating the magnitude of myocardium at risk and the extent of angiographic coronary artery disease: a <sup>82</sup>Rb PET/CT study. *J Nucl Med*. 2007;349–358.
32. Gould KL, Lipscomb K. Effects of coronary stenoses on coronary flow reserve and resistance. *Am J Cardiol*. 1974;34:48–55.
33. Di Carli M, Czernin J, Hoh CK, et al. Relation among stenosis severity, myocardial blood flow, and flow reserve in patients with coronary artery disease. *Circulation*. 1995;91:1944–1951.
34. Uren NG, Melin JA, De Bruyne B, Wijns W, Baudhuin T, Camici PG. Relation between myocardial blood flow and the severity of coronary-artery stenosis. *N Engl J Med*. 1994;330:1782–1788.
35. Beanlands RS, Muzik O, Melon P, et al. Noninvasive quantification of regional myocardial flow reserve in patients with coronary atherosclerosis using nitrogen-13 ammonia positron emission tomography: determination of extent of altered vascular reactivity. *J Am Coll Cardiol*. 1995;26:1465–1475.
36. Parkash R, deKemp RA, Ruddy TD, et al. Potential utility of rubidium 82 PET quantification in patients with 3-vessel coronary artery disease. *J Nucl Cardiol*. 2004;11:440–449.
37. Kuhle WG, Parenta G, Huang SC, et al. Quantification of regional myocardial blood flow using <sup>13</sup>N-ammonia and reoriented dynamic positron emission tomographic imaging. *Circulation*. 1992;86:1004–1017.
38. Nitzsche EU, Choi Y, Czernin J, Hoh CK, Huang SC, Schelbert HR. Noninvasive quantification of myocardial blood flow in humans: a direct comparison of the [<sup>13</sup>N]ammonia and the [<sup>15</sup>O]water techniques. *Circulation*. 1996;93:2000–2006.
39. Muzik O, Beanlands RS, Hutchins GD, Mangner TJ, Nguyen N, Schwaiger M. Validation of nitrogen-13-ammonia tracer kinetic model for quantification of myocardial blood flow using PET. *J Nucl Med*. 1993;34:83–91.
40. Lin JW, Laine AF, Akinboboye O, Bergmann SR. Use of wavelet transforms in analysis of time-activity data from cardiac PET. *J Nucl Med*. 2001;42:194–200.
41. Lin JW, Laine AF, Bergmann SR. Improving PET-based physiological quantification through methods of wavelet denoising. *IEEE Trans Biomed Eng*. 2001; 48:202–212.
42. El Fakhri G, Sitek A, Guerin B, Kijewski MF, Di Carli MF, Moore SC. Quantitative dynamic cardiac <sup>82</sup>Rb PET using generalized factor and compartment analyses. *J Nucl Med*. 2005;46:1264–1271.
43. El Fakhri G, Guerin G, Sitek A, et al. Absolute myocardial blood flow quantification in Rb-82 cardiac PET using generalized factor and compartment analysis: a reproducibility study. *Eur J Nucl Med Mol Imaging*. 2006;33:S217.
44. Yoshinaga K, Chow BJ, Williams K, et al. What is the prognostic value of myocardial perfusion imaging using rubidium-82 positron emission tomography? *J Am Coll Cardiol*. 2006;48:1029–1039.
45. Dorbala S, Hachamovitch R, Kwong R, Curillova Z, Di Carli MF. Incremental prognostic value of rubidium-82 myocardial perfusion PET-CT imaging in patients with known or suspected CAD. *J Am Coll Cardiol*. 2007;49:109A.
46. Dorbala S, Hachamovitch R, Kwong R, Curillova Z, Di Carli MF. Incremental prognostic value of left ventricular ejection fraction assessment over myocardial perfusion imaging: a rubidium-82 PET/CT study. *J Am Coll Cardiol*. 2007; 49:109A.
47. Di Carli MF, Dorbala S, Limaye A, et al. Clinical value of hybrid PET/CT cardiac imaging: complementary roles of multi-detector CT coronary angiography and stress PET perfusion imaging [abstract]. *J Am Coll Cardiol*. 2006; 47:115A.
48. Hacker M, Jakobs T, Matthiesen F, et al. Comparison of spiral multidetector CT angiography and myocardial perfusion imaging in the noninvasive detection of functionally relevant coronary artery lesions: first clinical experiences. *J Nucl Med*. 2005;46:1294–1300.
49. Schuijff JD, Wijns W, Jukema JW, et al. Relationship between noninvasive coronary angiography with multi-slice computed tomography and myocardial perfusion imaging. *J Am Coll Cardiol*. 2006;48:2508–2514.
50. Rispler S, Roguin A, Keidar Z, et al. Integrated SPECT/CT for the assessment of hemodynamically significant coronary artery lesions. *J Am Coll Cardiol*. 2007; 49:1059–1067.
51. Gould KL. Identifying and measuring severity of coronary artery stenosis: quantitative coronary arteriography and positron emission tomography. *Circulation*. 1988;78:237–245.
52. Leber AW, Knez A, von Ziegler F, et al. Quantification of obstructive and nonobstructive coronary lesions by 64-slice CT: a comparative study with quantitative coronary angiography and intravascular ultrasound. *J Am Coll Cardiol*. 2005;46:147–154.
53. Shaw LJ, Hachamovitch R, Berman DS, et al. The economic consequences of available diagnostic and prognostic strategies for the evaluation of stable angina patients: an observational assessment of the value of precatheterization ischemia—Economics of Noninvasive Diagnosis (END) Multicenter Study Group. *J Am Coll Cardiol*. 1999;33:661–669.
54. Di Carli MF, Hachamovitch R. The study of myocardial perfusion and coronary anatomy imaging roles in CAD (SPARC). Available at: <http://www.sparctrial.org>. Accessed April 2, 2007.